Supporting Information

Triple non-covalent dynamic interactions enabled tough and rapid room temperature self-healing elastomer for next generation soft antenna

Pengxiang Si, Fan Jiang, Qingsha S. Cheng, Geoffrey Rivers, Hongjie Xie, Aung Ko Ko Kyaw and Boxin Zhao**

P. Si, G. Rivers, B. Zhao
Department of Chemical Engineering
Waterloo Institute for Nanotechnology
Institute for Polymer Research
University of Waterloo
200 University Avenue West, N2L 3G1, Canada
E-mail: zhaob@uwaterloo.ca

F. Jiang, Q. S. Cheng, H. Xie, AKK. Kyaw
Department of Electrical and Electronic Engineering
Southern University of Science and Technology
1088 Xueyuan Ave, 518055, China
E-mail: chengqs@sustech.edu.cn

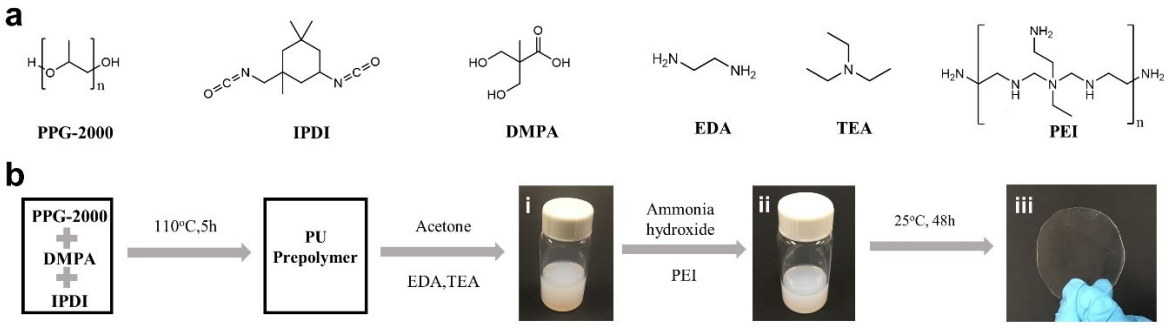

Fig S1. (a) Chemical structures of the compounds for synthesizing PU-PEI elastomer. (b) Schematic illustration of the fabrication of PU-PEI elastomer (i. PU colloid; ii. PU-PEI colloidal complex; iii. PU-PEI elastomer).

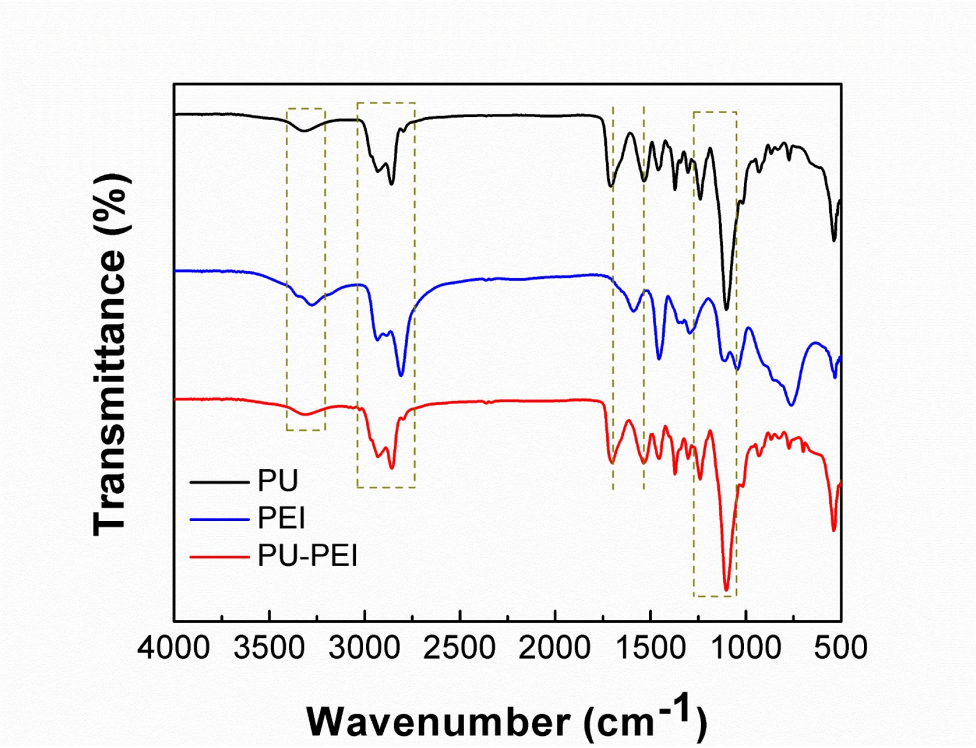

Fig S2. FTIR spectra of PU, PEI and PU-PEI.

The FTIR spectra of PU, PEI and PU-PEI are shown in Fig S2. The PU has typical peaks of N-H stretching at 3323 cm^{-1}, C-H stretching at 2937 cm^{-1} and 2860 cm^{-1}, C=O stretching at 1709 cm^{-1}, N-H bending at 1535 cm^{-1}, C-H bending at 1458 cm^{-1} and 1365 cm^{-1}, C-O stretching at 1235 cm^{-1} and 1102 cm^{-1}, and no absorption peak of the N=C=O group (2270 cm^{-1}), indicating the formation of urethane (H-N-COO-) group from N=C=O (IPDI) and O-H (PPG-2000). The PEI has typical peaks of N-H stretching at 3276 cm^{-1}, C-H stretching at 2940 cm^{-1} and 2806 cm^{-1} N-H bending at 1596 cm^{-1}, C-H bending at 1458 cm^{-1} and 1342 cm^{-1}, and C-N stretching at 1350–1000 cm^{-1}.[S1] The similar FTIR spectra for both PU and PU-PEI elastomers indicate that no chemical reaction occurred after incorporating PEI into PU.

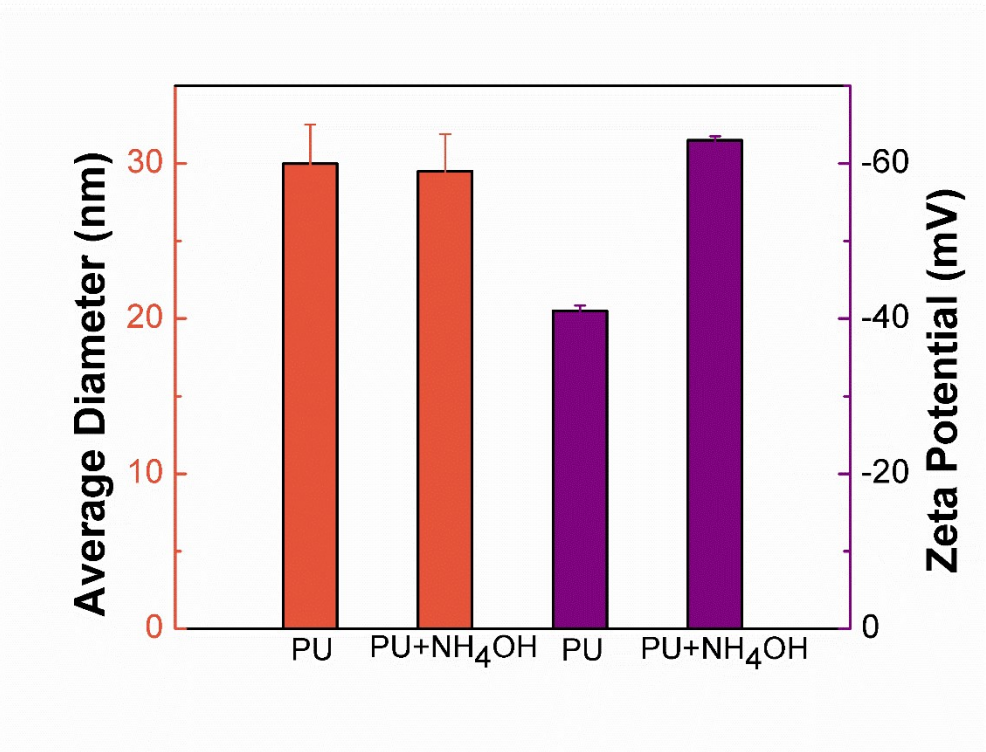

Fig S3. Average diameter and zeta potential of PU and PU-NH4OH colloid.

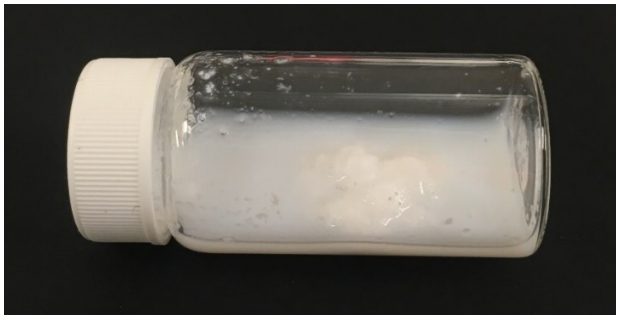

Fig S4. Precipitation of PU-PEI colloid complex without ammonia hydroxide protection.

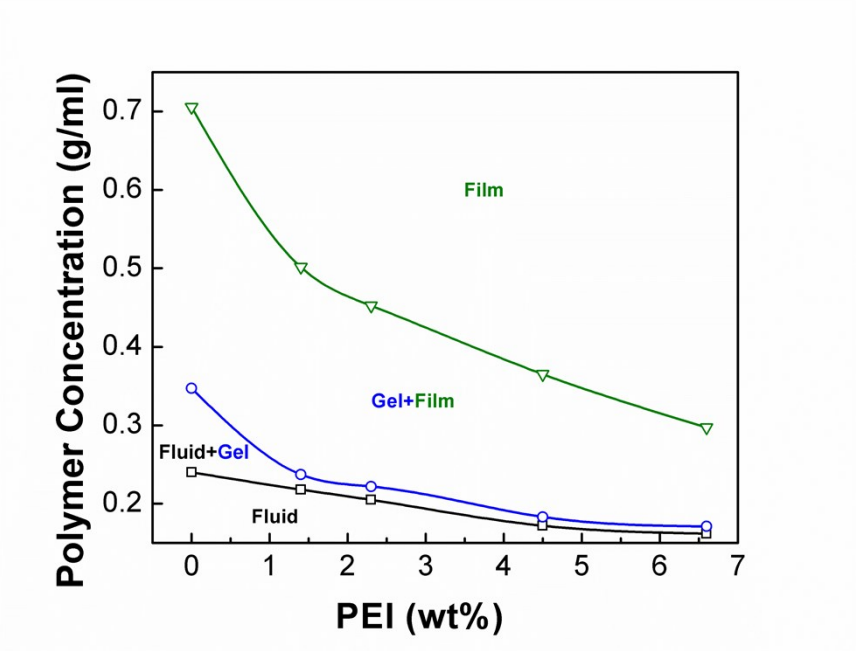

Fig S5. Phase behavior of PU-PEI colloidal complex with different initial concentrations (wt%) of PEI during the water evaporation.

As the water evaporated, the polymer concentration of PU-PEI colloidal complex increased, resulting in phase change from fluid to gelation and then film. Initially, the samples contain the PU colloidal particles and the PEI polymers, which exist as a stable fluid. As the concentration increases, samples start to aggregate without losing their flowability. The aggregation is whitish and can be readily noticed with naked eyes. Then, with the continuous evaporation of water, samples become a gel that cannot flow. In the gelation state, samples only have weak mechanical properties that has not formed a film yet. Finally, as the color turns from white to transparent, the gel becomes to a continuous film that can be peeled off.

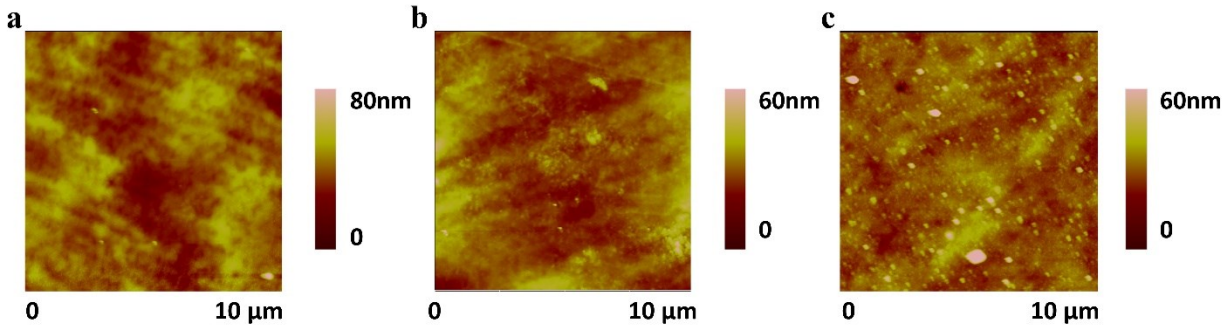

Fig S6. (a) AFM phase diagram of PU-PEI elastomer with (a) 0% PEI, (b) 2.3% PEI and (c) 6.6% PEI

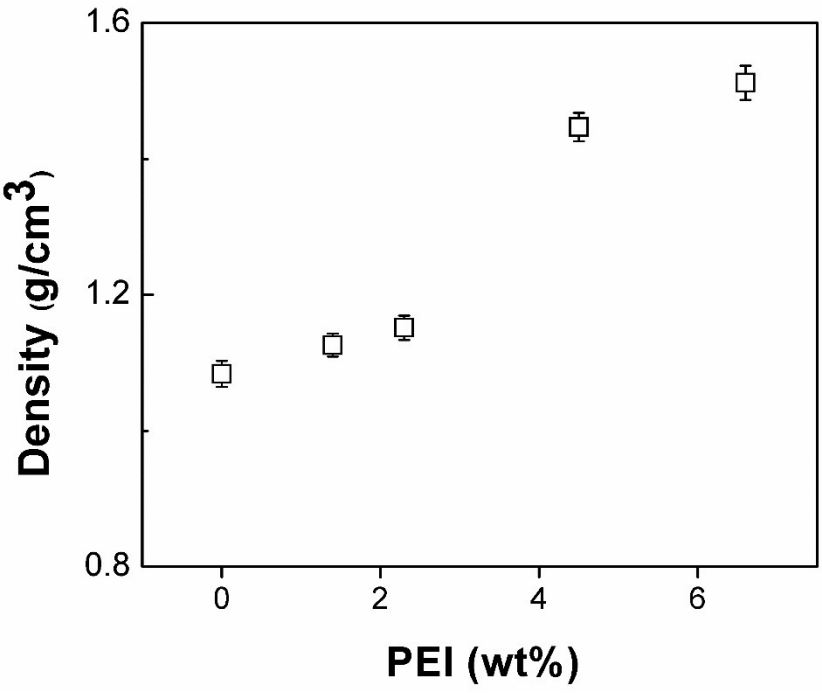

Fig S7. Measured density of PU-PEI elastomers with different concentrations of PEI.

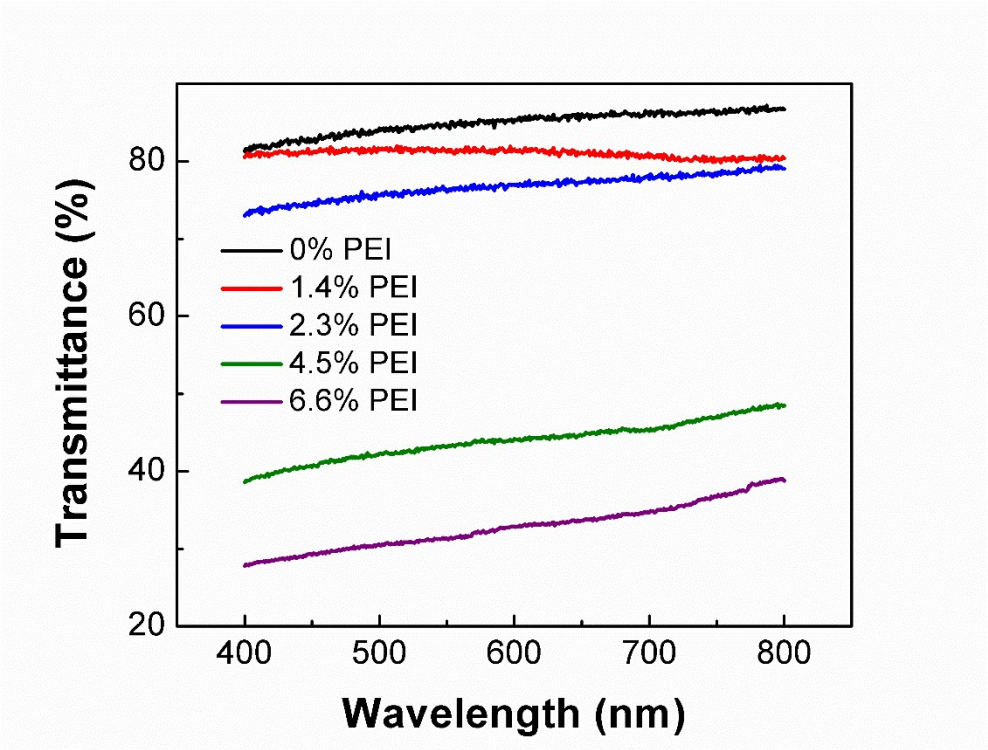

Fig S8. Transmittance of PU-PEI elastomers with different concentrations of PEI.

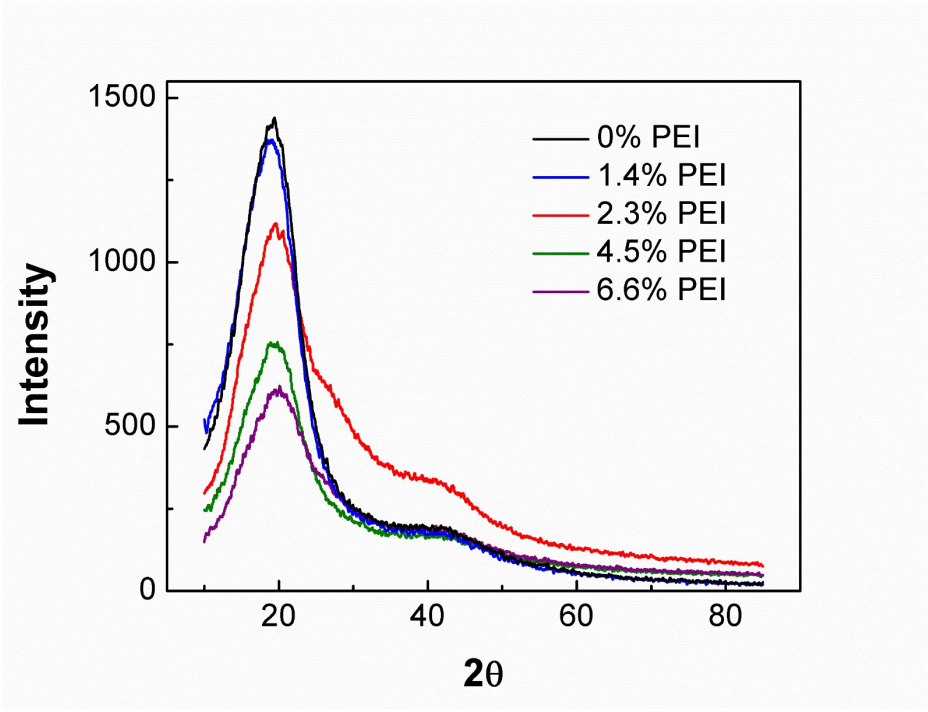

Fig S9. X-Ray diffraction of PU-PEI elastomers with different concentrations of PEI.

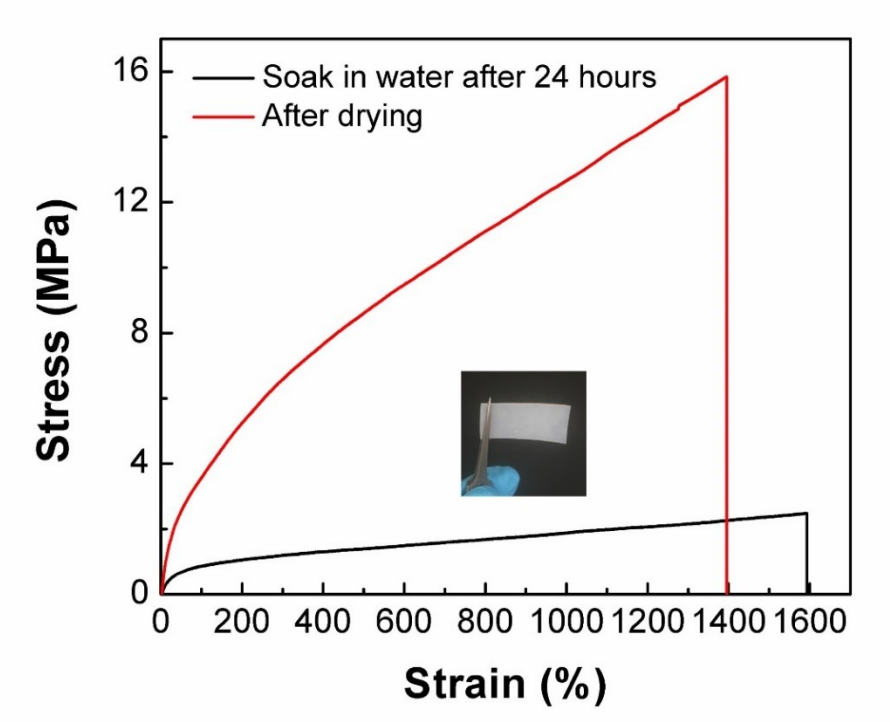

Fig S10. Stress-strain curve for PU-PEI elastomer (2.3% PEI) in wet and dry states. Inserted photo is PU-PEI elastomer (2.3% PEI) after soaking in water for 24 hours.

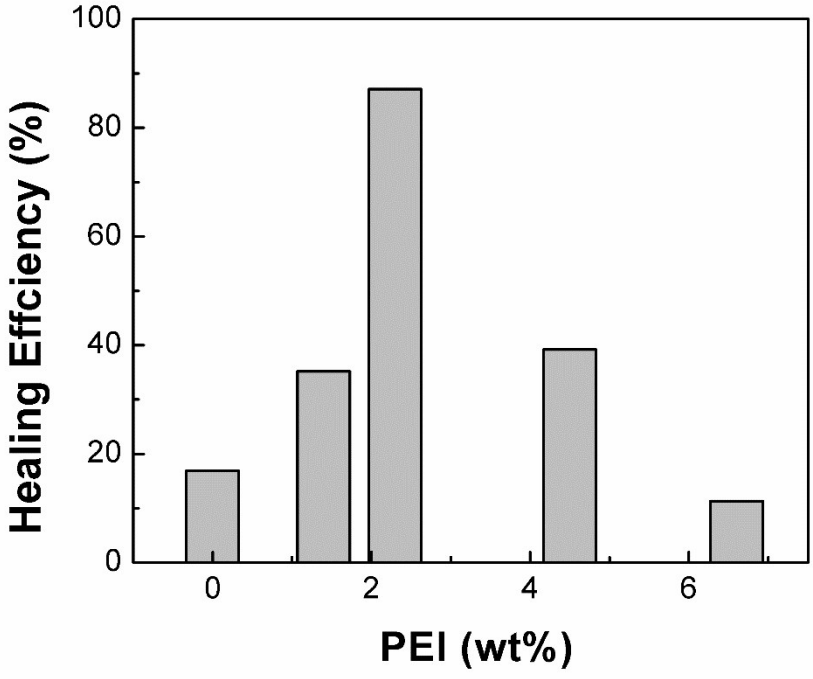

Fig S11. Self-healing efficiency of PU-PEI elastomers with different concentrations of PEI for 24 hours.

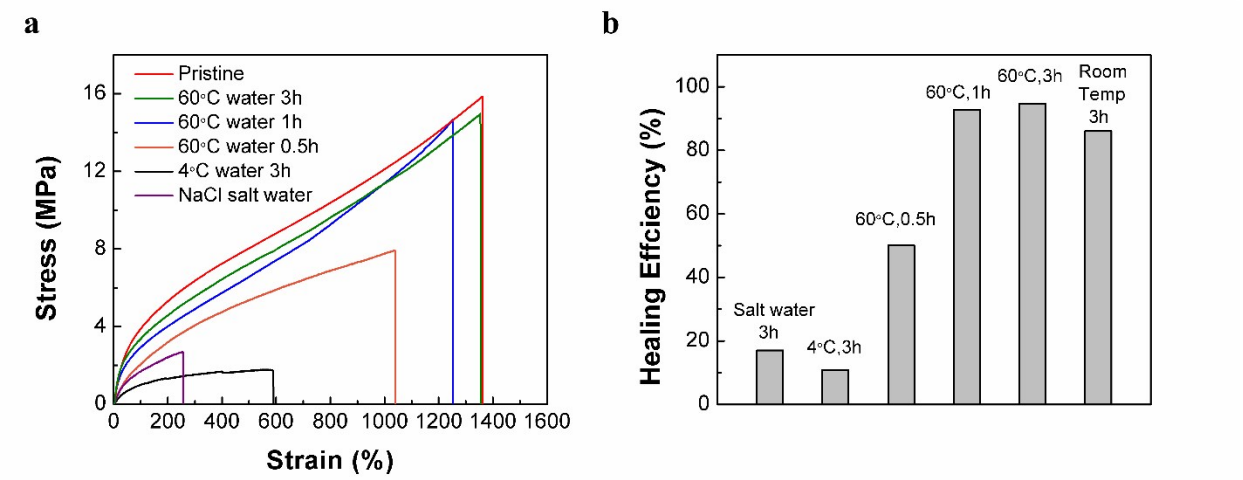

Fig S12. (a) Stress-strain curve of healed PU-PEI elastomer (2.3% PEI) at different healing conditions. (b) Self-healing efficiency of PU-PEI elastomers (2.3%PEI) at different healing conditions.

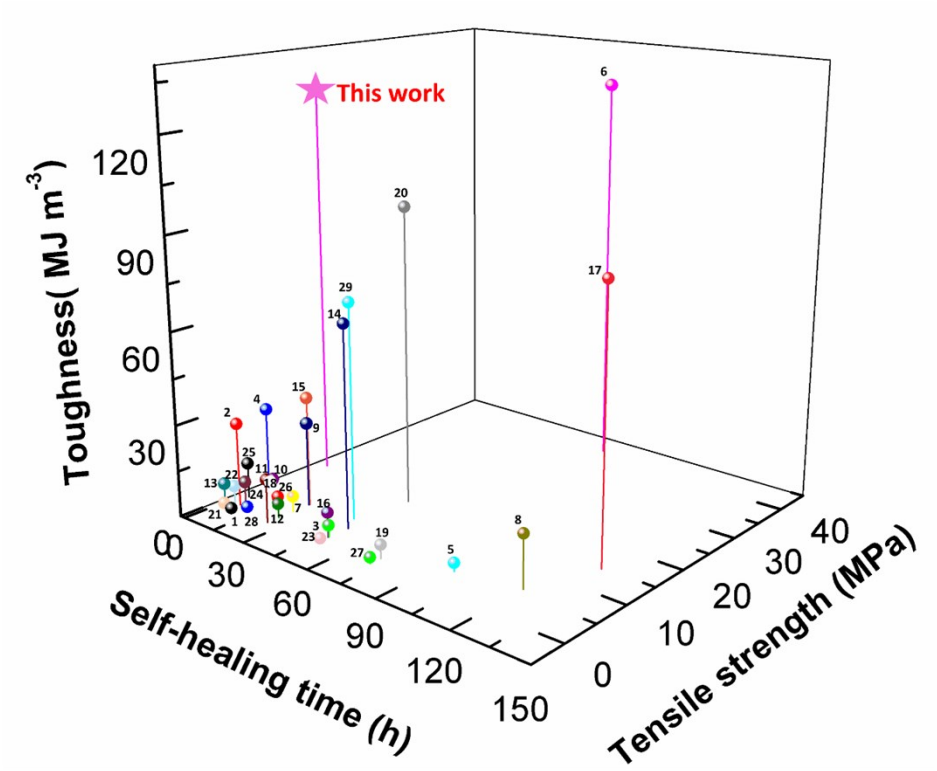

Covalent bond

1. Imine [Ref 32]
3. Diselenide [Ref 33]
4. Disulfide [Ref 26]
5. Boronic Ester [Ref 20]
8. Imide [Ref 36]
11. Acylhydrazone [Ref 39]
13. Urea [Ref 41]
18. Disulfide [Ref 45]
19. Boronic ester [Ref 46]
21. Olefin [Ref 48]
28. Urea [Ref 18]

Covalent & Non-covalent bond

6. Imine, hydrogen bond [Ref 34]
10. Disulfide, hydrogen bond [Ref 38]
15. Disulfide, hydrogen bond [Ref 43]
17. Dimethylglyoxime–urethane, metal-coordinated bond, hydrogen bond [Ref 27]

Non-covalent bond

2. Hydrogen bond [Ref 22]
7. Hydrogen bond, coordination Interaction [Ref 35]
9. Hydrogen bond [Ref 37]
12. Hydrogen bond, electrostatic interaction [Ref 40]
14. Hydrogen bond [Ref 42]
16. Metal-coordinated bond, hydrogen bond [Ref 44]
20. Metal-coordinated bond, hydrogen bond [Ref 47]
22. Metal–Ligand [Ref 49]
23. Metal–Ligand [Ref 50]
24. Host-guest [Ref 24]
25. Supramolecular assembly [Ref 51]
26. Hydrogen bond [Ref 52]
27. Metal–Ligand [Ref 53]
29. Ionic bond [Ref 25]
★ Hydrogen bond, ionic bond, polymer entanglement interaction [This work]

Fig S13. Ashby plot of "toughness", "tensile strength" and "self-healing time" of the PU-PEI elastomer and other room temperature self-healing elastomers reported in literatures. [18,20,22,24-27,32-53]

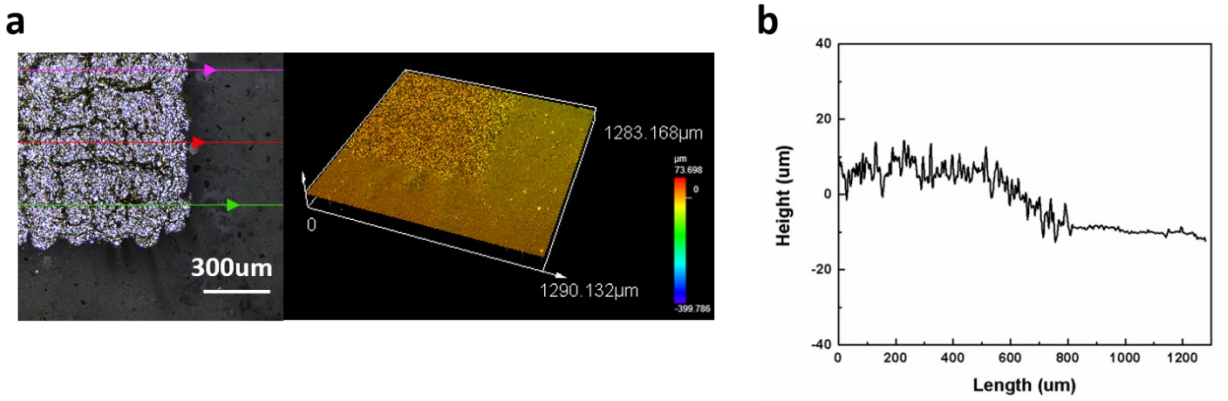

Fig S14. (a) Topology and (b) thickness of PU-PEI antenna.

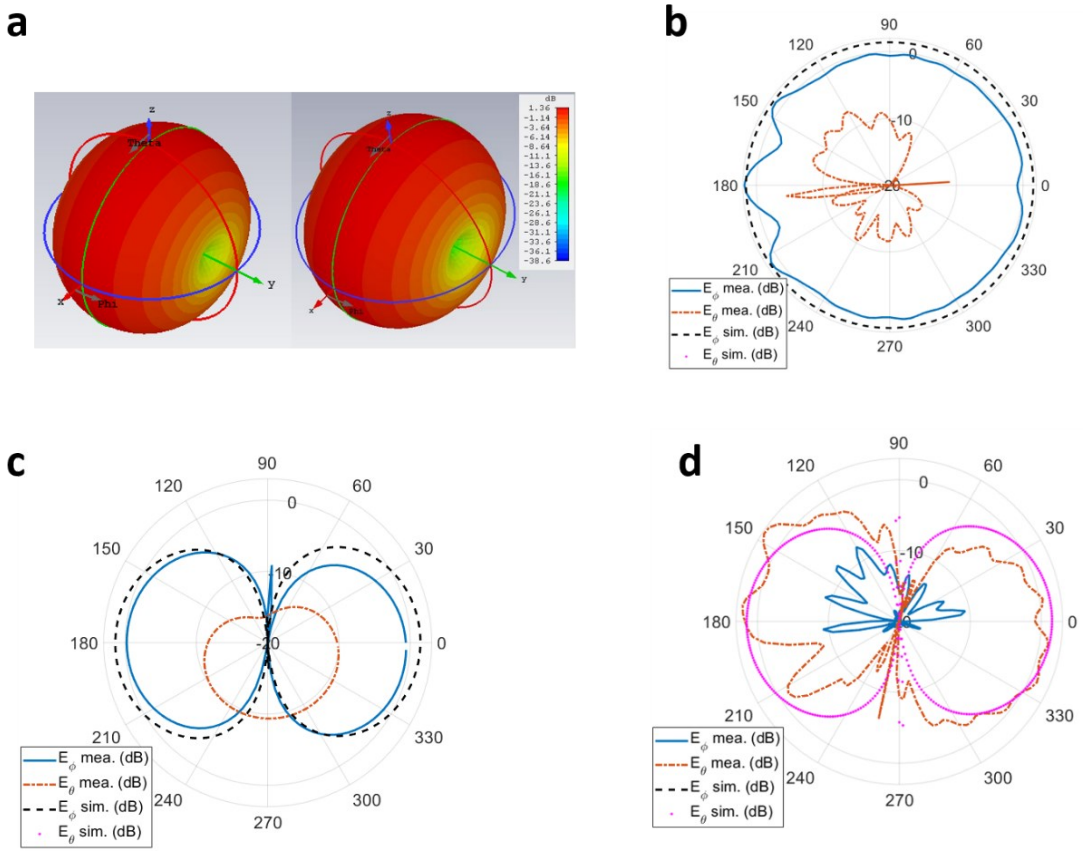

Fig S15. a) Simulated 3d radiation pattern of original (left) and healed (right) PU-PEI antenna. (b-d) Simulated and measured 2d radiation pattern of PU-PEI antenna at phi 0, theta 90 and phi 90, respectively.

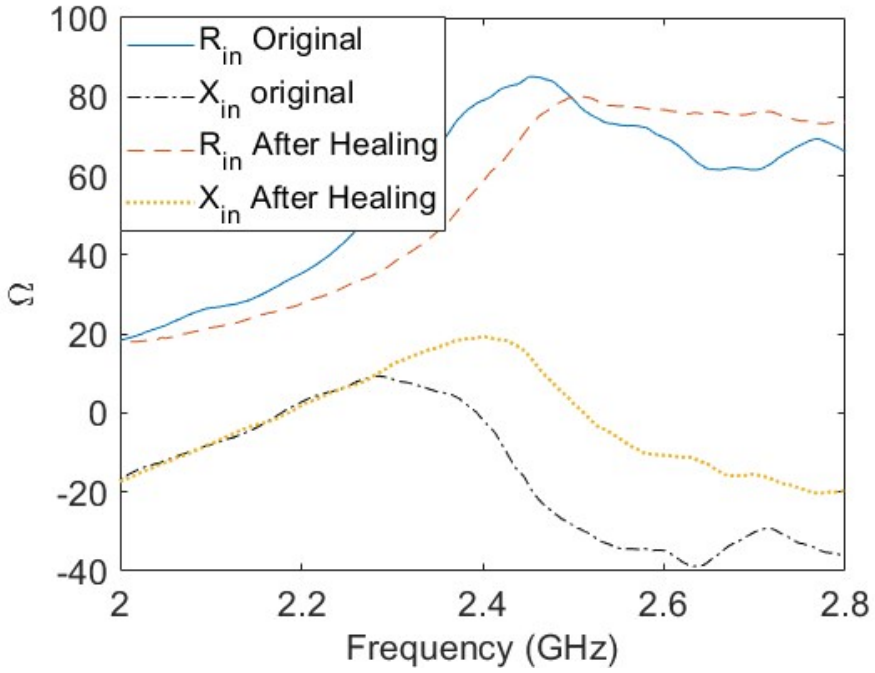

Fig S16. Measured impedance of original and healed PU-PEI antenna.

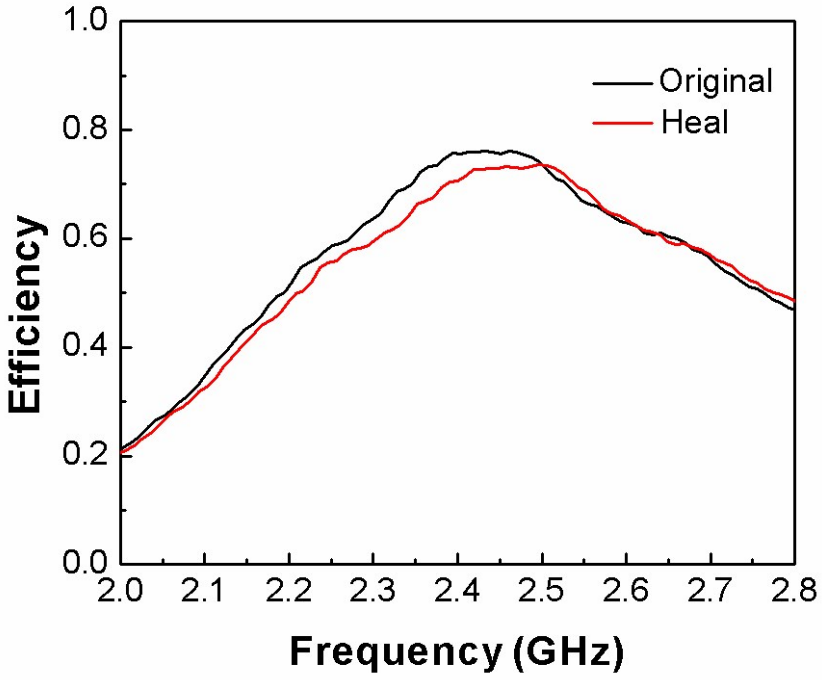

Fig S17. Effciency of original and healed PU-PEI antenna.

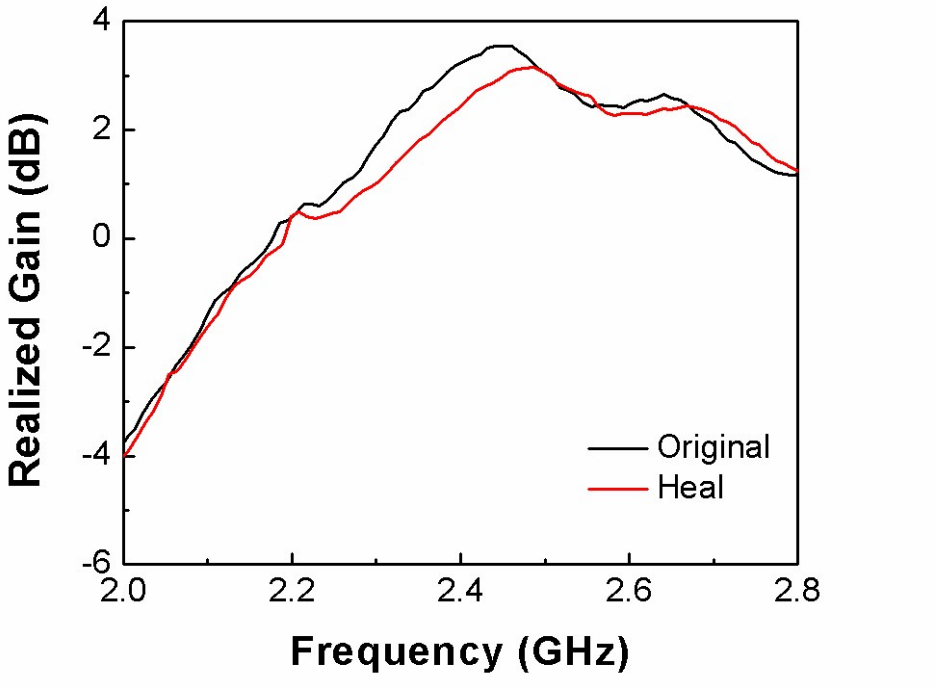

Fig S18. Realized gain of original and healed PU-PEI antenna.

Table S1. Comparison of electrical conductivity, stretchability and stretching cycles of the PU-PEI-Ag composite with other printable silver-based soft electronic materials.

Conductive components	Conductivity at 0% strain (S/cm)	Conductivity at 70% strain(S/cm)	Tested stretching cycles	Ref
Silver flake-carbon nanotube hybrid	5710	800	5000	S2
Silver flake	3570	1200	N/A	S3
Silver flake	738	400		S4
Silver nanoparticle	5450	3700	100	S5
Silver nanoparticle-carbon nanotube hybrid	6000	260	300	S6
Silver nanowire	16500	8002	1000	S7
Silver nanowire	2043	140	160	S8
Silver flake	4087	58	400	This work

References

S1. O. R. Pardini and J. I. Amalvy, *J. Appl. Polym. Sci.*, 2008, **107**, 1207–1214.

S2. K. Y. Chun, Y. Oh, J. Rho, J. H. Ahn, Y. J. Kim, H. R. Choi and S. Baik, *Nat. Nanotechnol.*, 2010, **5**, 853–857.

S3. T. Araki, M. Nogi, K. Suganuma, M. Kogure and O. Kirihara, *IEEE Electron Device Lett.*, 2011, **32**, 1424–1426.

S4. N. Matsuhisa, M. Kaltenbrunner, T. Yokota, H. Jinno, K. Kuribara, T. Sekitani and T. Someya, *Nat. Commun.*, 2015, **6**, 7461.

S5. M. Park, J. Im, M. Shin, Y. Min, J. Park, H. Cho, S. Park, M. B. Shim, S. Jeon, D. Y. Chung, J. Bae, J. Park, U. Jeong and K. Kim, *Nat. Nanotechnol.*, 2012, **7**, 803–809.

S6. R. Ma, J. Lee, D. Choi, H. Moon and S. Baik, *Nano Lett.*, 2014, **14**, 1944–1951.

S7. J. Liang, K. Tong and Q. Pei, *Adv. Mater.*, 2016, **28**, 5986–5996.

S8. H. W. Zhu, H. L. Gao, H. Y. Zhao, J. Ge, B. C. Hu, J. Huang and S. H. Yu, *Nano Res.*, 2020, **12**, 1–6.